Modulated and ordered defect structures in electrically degraded Ni–$BaTiO_3$ multilayer ceramic capacitors

G. Y. Yang,[a] E. C. Dickey, and C. A. Randall
Center for Dielectric Studies, Materials Research Institute, Department of Materials Science and Engineering, The Pennsylvania State University, University Park, Pennsylvania 16802

M. S. Randall and L. A. Mann
KEMET Electronics Corporation, 201 Fairview Street Extension, Fountain Inn, South Carolina 29644

(Received 9 June 2003; accepted 11 August 2003)

Structural defects formed on {111} planes of $BaTiO_3$ during the degradation of high performance multilayer Ni–$BaTiO_3$ X7R ceramic capacitors are studied using transmission electron microscopy and electron energy loss spectroscopy (EELS). Regular pseudocubic barium titanate grains are present in as-produced (virginal) base-metal electrode capacitors. However, there is a coexistence of regular, modulated, and long-range ordered structures in intentionally electrically degraded devices. The EELS analysis demonstrates that the concentration of oxygen vacancies in barium titanate with modulated or ordered structures is higher than that in the regular perovskite grains. The clustering or accumulation of oxygen vacancies in the structural framework of $BaTiO_3$ gives rise to the formation of new metastable structures. These observations are consistent with earlier models for degradation, but demonstrate that the details of the process may be more complex than originally assumed. Here we introduce new details on the nature of the reduction process and the manner in which the lattice accommodates the enhanced oxygen vacancy concentration towards the failed regions of the capacitors and in the vicinity of the ''blocking'' cathodic electrodes. © *2003 American Institute of Physics.* [DOI: 10.1063/1.1615300]

I. INTRODUCTION

$BaTiO_3$ is widely used as a dielectric in multilayer ceramic capacitors (MLCCs). Through chemical additions it is suitably formulated to control the temperature coefficient of capacitance and degradation resistance.[1] This study concerns X7R-type dielectrics having a $\pm 15\%$ change in capacitance between -55 and 125 °C from the 25 °C capacitance value. To reduce the cost of MLCCs while maintaining device performance, precious-metal internal electrodes (PME) are replaced with base metal electrodes (BME). The best candidate for such a replacement is found to be nickel.[2–4] It is necessary to cofire the Ni electrodes and $BaTiO_3$ dielectrics in reducing atmospheres to avoid oxidation of the electrode. Consequently, and despite acceptor doping of the dielectrics, a large number of oxygen vacancies are accommodated in $BaTiO_3$ when the capacitors are fired at low oxygen partial pressures. The long-time failure mechanism of BME MLCCs is thought to be dominated by the electromigration of oxygen vacancies.[5,6] Grain boundaries limit transport of oxygen vacancies across the bulk of the dielectric and thus retard the degradation process. Additionally, the electrode interface is key in the control of degradation rates as it controls the electron injection at the cathode.[7] Segregation of acceptor dopants and amphoteric dopants is important in limiting the migration of the vacancies across and along grain boundaries. Amphoteric dopants are ions that can easily occupy both Ba sites and Ti sites in the perovskite $BaTiO_3$ crystal lattice to act as donor or acceptor dopants, respectively. These both buffer and limit second phase stability at high temperatures and also aid in the Schottky barrier development at interfaces during the reoxidation process.[8–10]

In general, ABO_3 perovskites demonstrate a strong ability to accommodate a large number of oxygen vacancies and maintain a regular pseudocubic structure. It has been found that superstructures associated with ordered oxygen vacancies, such as the well-characterized brownmillerite structure, are formed in some oxygen-deficient perovskite oxides.[11–15] It has been also observed that microstructural defects in $BaTiO_3$, such as growth twins or microtwins with {111} planar interfaces, are correlated to the oxygen vacancies in $BaTiO_3$.[16,17] In the $BaTiO_3$ unit cell, the small titanium ion is located at the center of the oxygen octahedron. Each octahedron shares each of its corners with another octahedron. The large barium ion is at the central position of the space surrounded by eight oxygen octahedra in 12-fold coordinated sites. The stacking sequence is of one BaO_3 (111) plane followed by one Ti (111) plane. It has been suggested by the combination of experimental observations and theoretical simulations of high-resolution transmission electron microscopy (TEM) (HRTEM) images that {111} planar defects are associated with oxygen deficiencies in the {111} planes of the $BaTiO_3$ lattice. The oxygen vacancies in the Ba–O_3 composition plane may be accompanied by a change in the oxidation state of the nearest-neighbor Ti ions from a higher valence to a lower valence in order to maintain the local electrostatic charge balance.[16]

The potential impact of oxygen nonstoichiometry on $BaTiO_3$-based dielectrics has stimulated research on the pro-

[a]Electronic mail: gxy10@psu.edu

cessing and characterization of BME ceramic capacitors as the devices are fired and reoxidized in relatively low PO_2 atmospheres.[18] It is believed that the gradual time-dependent decrease in insulation resistance of dielectric ceramics under simultaneous temperature and dc electrical field stresses may be explained by the net electromigration of oxygen vacancies toward the cathode due to the positive charge of oxygen vacancies with respect to the regular lattice.[6,19,20] Investigations of the time-dependent insulation resistance degradation in $BaTiO_3$-based BME MLCC systems with amphoteric doping, acceptor doping, and reoxidation have all been reported by a number of researchers.[2,3,8,9,18] Generally, it is suggested that before the highly accelerated life test (HALT), the oxygen vacancies are randomly distributed within the dielectric layers. However, there may be local influences, such as the case of core-shell X7R dielectrics, where there may be higher oxygen vacancy concentrations in the cores.[18] During HALT testing, positively charged oxygen vacancies redistribute and move towards the cathode. In this article, we report on a study of microstructural and microchemical changes observed during the degradation process. Planar defects on the {111} planes of barium titanate that are associated with clustering or long-range ordering of oxygen vacancies in the basic structural framework of the perovskite lattice in commercial BME X7R ceramic capacitors are reported.

II. EXPERIMENTAL PROCEDURES

$Ni/BaTiO_3$ BME MLCCs were produced via a standard multilayer process utilizing screen printing of $Ni/BaTiO_3$ tapes, lamination, debinding organics, and cofiring at $\sim$1300 °C in a PO_2 of $\sim 10^{-10}$ atm followed by an annealing at $\sim$800 °C in a PO_2 of $\sim 10^{-8}$ atm. HALT tests were then performed on the BME MLCCs to induce degradation in the insulation resistance of the capacitors. The parts were then evaluated by measuring the complex impedances before and after exposure to applied voltages of 1–5 V at 325 °C in N_2. The N_2 was added to prevent oxidation of the copper termination during measurement.

It is known that the degradation in insulation resistance of $Ni/BaTiO_3$ capacitors can be inhomogeneously and locally distributed throughout the devices.[21] In order to realize TEM observation and EELS analysis on strongly degraded regions of the capacitors, scanning electron microscopy-voltage contrast (SEM-VC) imaging was used to locate the failed area (or areas) in the capacitors.[22] SEM-VC was performed with an acceleration voltage of 2 kV to minimize the secondary electron imaging effect. Figure 1 shows a typical SEM-VC image of a $Ni/BaTiO_3$ capacitor. The internal electrodes identified as A and B (anode and cathode) are noted by the arrows. Brightness crossing the electrode in Fig. 1 is an indication of the degradation in insulation resistance of the dielectric. A stronger dependence of the image contrast with respect to applied dc potential was observed near the tips of the B electrodes in some cases and is an indication of conduction associated with a relatively high local concentration of oxygen vacancies, which leads to enhanced semiconducting behavior.

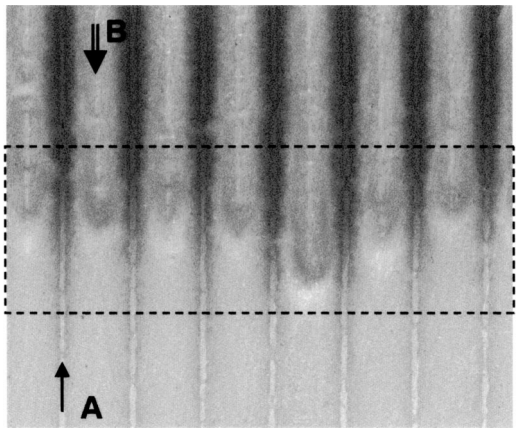

FIG. 1. Voltage contrast SEM image of $Ni/BaTiO_3$ capacitors. The dependence of the image contrast on the applied dc potential near the tips of the B electrodes is indicative of conduction.

Cross sectional TEM samples were prepared following traditional procedures including mechanical polishing and ion milling. Ion milling was performed using a Fishione Model 3000 Ion Mill operated at 4 to 5 kV and 5 mA with an inclination angle of 10°–12° to produce electron transparent foils. The samples were cooled to liquid-nitrogen temperature during ion milling to minimize possible structural damage and artifacts.

Electron diffraction, TEM, and HRTEM observations were all performed using a JEOL 2010F transmission electron microscope equipped with a field-emission gun operated at 200 kV. The experiments for the failed capacitors were carried out within or near the region noted by the rectangle shown in Fig. 1.

Electron energy loss spectroscopy (EELS) analysis was carried out using a Gatan Enfina parallel electron energy-loss spectrometer attached to the JEOL 2010F TEM. The energy resolution measured by the zero-loss peak was about 1.1 eV full width at half maximum (FWHM). Electron energy loss spectra were recorded in TEM-diffraction mode with a collection angle of 14 mrad. The spectra including the Ti $L_{2,3}$ and O K edges were recorded from a number of $BaTiO_3$ grains with the incident electron beam 2° to 3° away from the $[10\bar{1}]$ zone axis of the pseudocubic $BaTiO_3$ crystal structure to avoid electron channeling-enhanced effects. After appropriate background subtraction, the Ti/O ratio was extracted by integrating the respective edges over an energy window of about 22 eV and obtaining an edge count ratio. The chemical compositions of the individual grains were quantified using a K-factor (or sensitivity factor) approach using an air-processed barium titanate in precious metal electrode (PME) capacitors as a standard, which were believed to be fully stoichiometric.

III. RESULTS AND DISCUSSION

Structural imperfections in $BaTiO_3$ dielectric grains are frequently observed in the degraded BME MLCCs as evidenced by the appearance of additional reflections in the electron diffraction patterns. Figures 2(a)–2(d) show four selected-area electron diffraction (SAED) patterns taken

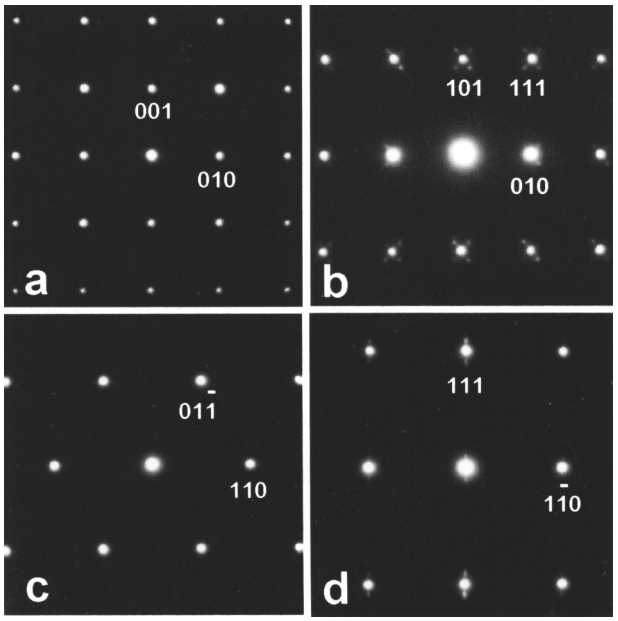

FIG. 2. SAED patterns obtained from different $BaTiO_3$ grains. Patterns (a) and (c) are indexed as the [100] and $[\bar{1}\bar{1}1]$ zone axes of pseudocubic perovskite structure. The presence of satellite spots in patterns (b) and (d), indexed as the $[10\bar{1}]$ and $[\bar{1}\bar{1}2]$ zone axes, indicates structural modulation.

from the $BaTiO_3$ grains. The diffraction patterns are indexed as the [100], $[10\bar{1}]$, $[\bar{1}\bar{1}1]$, and $[\bar{1}\bar{1}2]$ zone axes of the pseudocubic perovskite structure, respectively. In addition to the basic reflections of the perovskite, satellite spots appear in the diffraction patterns of the $[10\bar{1}]$ and $[\bar{1}\bar{1}2]$ zone axes, in which {111} reflections are present. The appearance of such satellites spots in the ⟨111⟩ directions is associated with modulation in structure and/or chemistry of the material.[23] It should be noted that this kind of planar defect is not observed in as-produced or undegraded (virginal) BME capacitors. Therefore the following studies concerned with the microstructural imperfections of $BaTiO_3$ in Ni–$BaTiO_3$ MLCCs are performed with the incident electron beam parallel to the $[10\bar{1}]$ zone axis of pseudocubic perovskite structure on degraded grains.

It is shown in this work, through TEM and SAED analyses, that planar defects associated with a modulated structure in the {111} planes are the major defects in the $BaTiO_3$ dielectrics in the degraded Ni–$BaTiO_3$ MLCCs. These defects are distinct from the {111} twins and microtwins that have been frequently observed in $BaTiO_3$ powders,[24] sintered bulk $BaTiO_3$,[16,25] and films.[26–31] The {111} twins in $BaTiO_3$ are typically considered to be growth twins. The structural modulation observed in the degraded BME capacitors differs from these twins. Figure 3 shows a bright-field TEM micrograph of a $BaTiO_3$ grain in a degraded specimen. A variation in image contrast is observed from regions A to B. A ''wavy'' image contrast parallel to the {111} planes is observed in region B. The inserts in Fig. 3 are the SAED patterns obtained from regions A and B. The reflections in the diffraction pattern taken from region A are indexed as the basic reflections of a pseudocubic $BaTiO_3$, indicative of a regular perovskite structure. However, additional satellite spots near

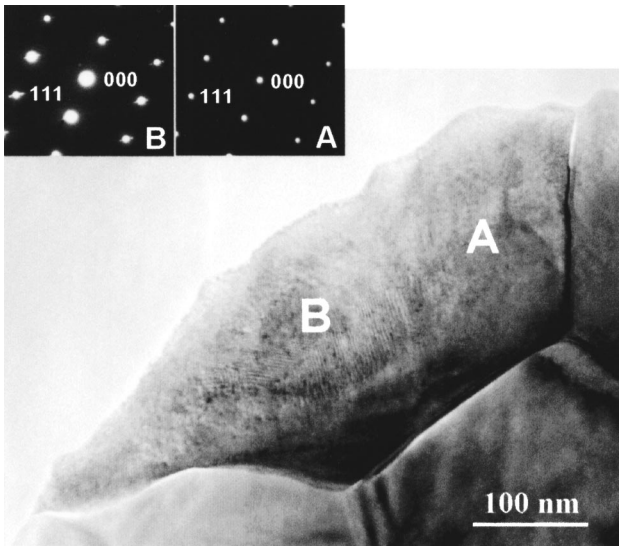

FIG. 3. Bright-field TEM micrograph of a $BaTiO_3$ grain in the degraded BME capacitor. Region A corresponds to the regular perovskite crystal structure and region B to that with structural modulation in the {111} planes.

{111} reflections of the perovskite appear in the electron diffraction patterns obtained from region B, indicating a modulated structure in region B. The complex image contrast in region B is correlated with the structural modulation on the {111} planes.

TEM observations indicate that the regular perovskite structure is maintained in some grains or grain regions. Figure 3 shows a mixture of regular and modulated structures. Figure 4(a) shows another bright-field TEM image of a single-crystal $BaTiO_3$ grain in which there exists a mixture of regular perovskite, modulated (region B), and long-range ordered structures (region C). The SAED patterns taken from regions B and C are shown in Figs. 4(b) and 4(c). The network-like structure in region B is associated with a modulated structure of the dielectric, which correlates with the satellite spots in the corresponding electron diffraction pattern [Fig. 4(b)]. The satellites in Fig. 4(b) are present in the

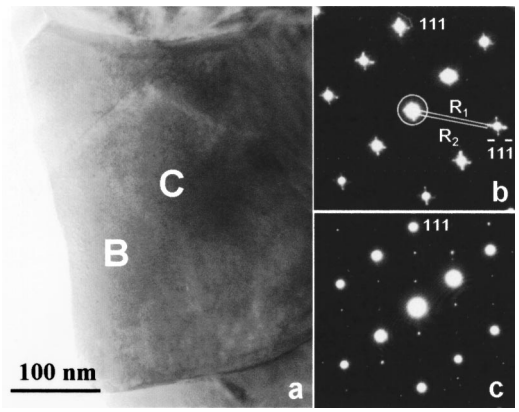

FIG. 4. (a) Bright-field image of the degraded $BaTiO_3$ dielectric showing the mixture of the regular perovskite, modulated (region A), and long-range ordered structures (region B). (b) and (c) are the SAED patterns taken from regions A and B. The patterns are indexed as the $[10\bar{1}]$ zone axis of the pseudocubic perovskite structure.

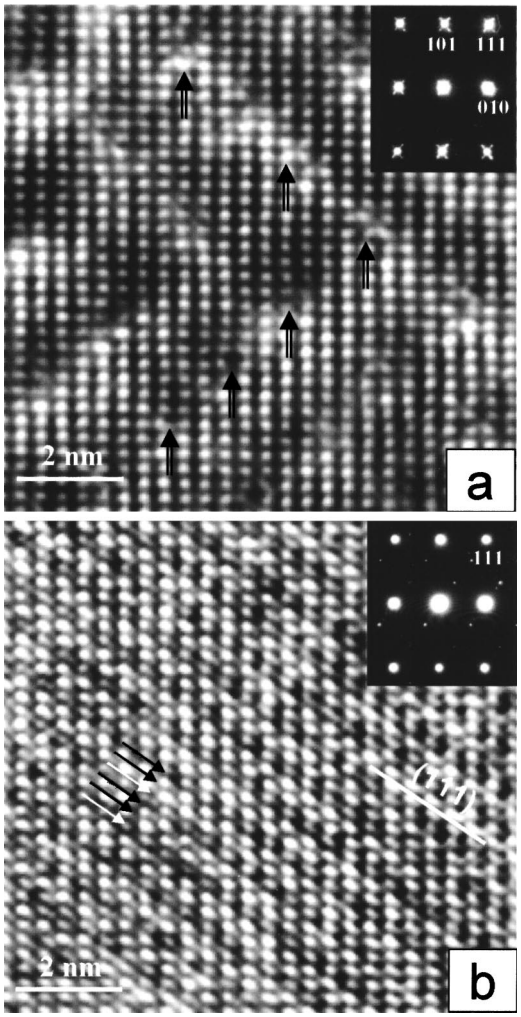

FIG. 5. HRTEM images of the modulated (a) and the long-range ordered structures (b) of degraded barium titanate. The insets are the corresponding SAED patterns.

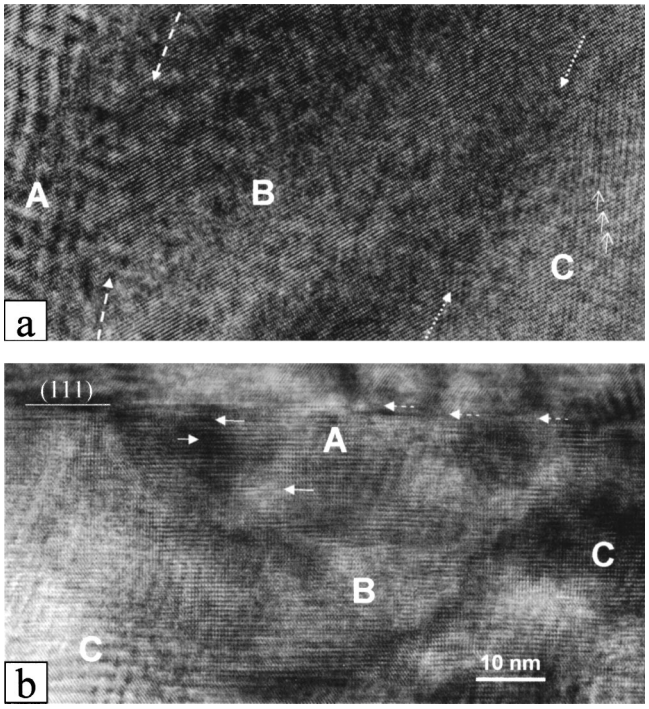

FIG. 6. HRTEM images of the mixture of regular perovskite, modulated, and long-range ordered structures (a) and copresence of modulated and long-range ordered structures (b) of $BaTiO_3$ in the degraded BME MLCC.

[111] and the $[\bar{1}\bar{1}\bar{1}]$ directions. R_1 and R_2 represent the distances between the central spot and the {111} basic reflections and the satellites, respectively. Analysis performed on several barium titanate grains shows that the ratio $R_1/(R_1-R_2)$ ranges from 8 to 12, implying that the structural modulation occurs every 8 to 12 {111} crystallographic planes. However, the additional spots appear in the form of superlattice reflections in the electron diffraction pattern taken on region C [Fig. 4(c)], which is indicative of a commensurate long-range ordered structure. The evolution of the SAED pattern from the satellite spots to the superlattice reflections in the ⟨111⟩ directions shows that the structural modulation converts into a periodic structural ordering. The periodicity of three times the {111} interplanar distance ($3d_{111}$) was determined by the locations of the superlattice reflections in the diffraction pattern. The ordering is two-dimensional in the {111} planes in the degraded $BaTiO_3$ unit cell because the satellites are only present in the [111] direction in Fig. 4(c).[32]

Figures 5(a) and 5(b) show HRTEM images of the modulated and the long-range ordered structures of degraded barium titanate. The insets are the corresponding SAED patterns. The patterns are indexed as the $[10\bar{1}]$ zone axis of the regular perovskite. Shown in Fig. 5(a) is a HRTEM image of $BaTiO_3$ with the modulated structure. The lattice distortion noted by the arrowheads may be attributed to locally high lattice strains. As the satellites are in the ⟨111⟩ directions, the structural modulation occurs on the {111} planes of the $BaTiO_3$ grain, i.e., the network-like changes in image intensity are due to the modulation in microstructure and/or microchemistry in the $BaTiO_3$ lattice. The spacing between adjacent modulated planes is about 8–10 interplanar distances of {111} planes, which is consistent with the ratio of $R_1/(R_1-R_2)$ in Fig. 4. Shown in Fig. 5(b) is a HRTEM image of the long-range ordered structure in the dielectric. The image intensity in every third (111) plane (indicated by white arrows) is changed significantly. The stacking sequence in the [111] direction is associated with the long-range ordered structure with the periodicity of $3d_{111}$ revealed by electron diffraction (see the inset).

The long-range ordered structure coexists most often with the modulated structure in barium titanate grains in the degraded capacitors. Two typical cases of the mixture are studied using HRTEM (Fig. 6). In the case shown in Fig. 6(a) three kinds of image contrast are present. The region noted by letter A shows the typical structure characteristic of the modulated phase in Fig. 5(a). The changes in image intensity due to the structural modulation become faded in region B. Region B is most likely a regular $BaTiO_3$ perovskite region. Long-range ordered structure is shown in region C where the white arrows note the third (111) plane [as in Fig. 5(b)]. These results show that the microstructure of the dielectric varies locally even within individual barium titanate grains. The HRTEM image shown in Fig. 6(b) illustrates another

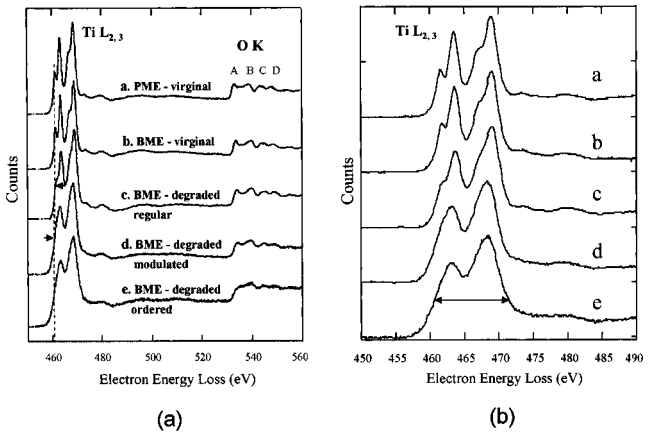

FIG. 7. (a) Ti $L_{2,3}$ and O K edges of barium titanate in the as-produced precious metal internal electrodes (PME) capacitors, as-produced BME capacitors, and in the degraded BME capacitors. (b) Enlarged part of Ti $L_{2,3}$ edges in (a) showing the $L_{2,3}$ peak width increase with lowering oxidation states of the dielectric grains.

TABLE I. Measured electron energy loss edge onset of L_3 for Ti $L_{2,3}$, Ti $L_{2,3}$ peak width, and oxygen content in barium titanate.

Materials	Ti L_3 edge onset (eV)	Measured Ti $L_{2,3}$ peak width (eV)	$BaTiO_x$
$BaTiO_3$ in PME capacitor	461.3 ± 0.1	9.1 ± 0.1	$BaTiO_{3.00\pm0.06}$
$BaTiO_3$ in BME capacitor	461.4 ± 0.1	9.1 ± 0.1	$BaTiO_{2.93\pm0.06}$
$BaTiO_3$ in degraded BME capacitor: regular barium titanate	461.4 ± 0.1	9.4 ± 0.1	$BaTiO_{2.86\pm0.06}$
$BaTiO_3$ in degraded BME capacitor: barium titanate modulated	460.7 ± 0.1	10.0 ± 0.1	$BaTiO_{2.60\pm0.06}$
$BaTiO_3$ in degraded BME capacitor: barium titanate ordered	460.6 ± 0.1	10.9 ± 0.1	$BaTiO_{2.60\pm0.06}$

case where the modulated phase and the ordered phase are present in one grain. Region A contains the long-range ordered phase. Planar defects are found on (111) planes and are noted by the arrows with solid lines. The ordered phase of about 50 nm in size is surrounded by an adjacent modulated phase, as noted by letter C. The image contrast in region B shows the character of both modulated and ordered structures, which might be due to the superposition of the ordered region on the surrounding modulated region along the incident electron beam direction. A faceted (111) twin plane (noted by the arrows with dashes) is also observed in the figure, although the {111} twin is not the major planar defect observed in the current work.

Considering the experimental observations that these defects preferentially occur in the degraded BME capacitors, it is likely that the local stoichiometry of the barium titanate is affected by electromigration of oxygen vacancies. The formation of oxygen vacancies in the {111} $Ba-O_3$ planes could be accompanied by a change in the oxidation state of the nearest-neighbor Ti ion from the ideal Ti^{4+} to a lower valence (Ti^{3+} or Ti^{2+}) in order to maintain the local charge balance of the dielectric. EELS is used to study the local stoichiometry and the oxidation state of the Ti ions in the degraded BME capacitors.

Figure 7(a) shows Ti $L_{2,3}$ edges and O K edges of barium titanate in the reference as-produced or undegraded (virginal) PME capacitors, as-produced (virginal) BME capacitors, and in the degraded BME capacitors. PME capacitors are considered close to stoichiometric as they were sintered in air. The spectrum (a) taken from the $BaTiO_3$ in PME capacitors is therefore used as a reference to quantify spectra (b)–(e) obtained from different capacitors and/or different regions in an identical device. The spectrum (b) was obtained from a dielectric grain in an as-produced $Ni-BaTiO_3$ capacitor and the spectra (c)–(e) from the degraded $Ni-BaTiO_3$ capacitor. The spectrum (c) was taken from the regular perovskite grain and spectra (d) and (e) were from the modulated and ordered regions, respectively. The lowest energy peak is the Ti L_3 edge (initial state $2p_{3/2}$) and the next is the Ti L_2 edge (initial state $2p_{1/2}$). The oxygen K edge contains a series of peaks labeled as A–D.[33,34] The atomic ratio of titanium and oxygen is determined by integrating the counts under the Ti $L_{2,3}$ and O K peaks. It is reasonable to consider that the barium titanate in a PME capacitor is close to that of a stoichiometric $BaTiO_3$, at least within the error of the measurement. The oxygen content in different dielectric grains is determined using the atomic ratio of $BaTiO_3$ in the PME multilayer capacitors as a reference. The calculated stoichiometries of the barium titanate are listed in Table I. The defect-free barium titanate gains in both the virginal and degraded BME multilayer capacitors indicate oxygen deficiency. Although the ABO_3 perovskite lattice is maintained, the concentration of the oxygen vacancies is further increased in the dielectric grains that exhibit the modulated and ordered structures. These experimental results show that highly defective dielectric grains contain an excess of oxygen vacancies that results in a structural transition from a regular perovskite lattice to a modulated and then ordered perovskite crystal structure.

The deficiency in oxygen anions could have a significant influence on the local cation valence. In $BaTiO_3$, the Ba cation may not be easily modified because it is more stable than the Ti cation, i.e., the BaO configuration is not expected to be affected. Analysis therefore concentrates on the Ti $L_{2,3}$ energy loss near edge structure (ELNES) which is dominated by atomistic effects, resulting in ''white-lines'' arising from transitions of $2p$ core electrons into the empty Ti $3d$ levels.[35] Apparent fine structure changes are observed in Fig. 7 when comparing spectra shown in Fig. 7(a). The $L_{2,3}$ edges are clearly split in the spectrum taken from the reference $BaTiO_3$ dielectric that is considered to be stoichiometric in Ti and O content. The splitting of the L_2 and L_3 edges is attributed to the crystal-field splitting of the t_{2g} and e_g molecular orbitals.[36,37] The sharp splitting of t_{2g} becomes a shoulder-like shape in spectrum (c), indicating a perturbation to the Ti–O octahedral coordination. The broadening of fine-structural lines is also associated with the valence decrease of the titanium ions.[38] The fine structures of the Ti $L_{2,3}$ edges in spectra (d) and (e) are different from spectra (a)–(c). The

most significant change is the disappearance of the splitting of the L_3 and L_2 peaks in the spectra taken from the regions where the modulated structure and/or long-range ordered structure are present. Titanium ions in barium titanate are octahedrally coordinated to oxygen as in rutile. The evolution in fine structure of the Ti $L_{2,3}$ edge from spectra (a)–(e) is similar to published ELNES from TiO_2 as it is successively reduced to Ti_2O_3 and TiO.[39,40] It is worth pointing out that the $e_g - t_{2g}$ splitting arises through orbital interactions between the Ti $3d$ and oxygen atoms: the spectra (a)–(c) correspond to the case where a gap exists between the e_g and t_{2g} bands and spectra (d) and (e) to the case where e_g and t_{2g} bands may overlap.[41]

The crystal-field effect is also reflected in the fine structure peaks just above the O *K* edge onset (peaks A and B) in Fig. 7(a). The general shapes of the O *K* edges are not significantly different from spectra (a) to (c). The intensity of peak A in spectra (d) and (e) is reduced compared with peak B. The decrease in peak A is caused by lattice distortion in linear Ti–O bonds in the perovskite structure due to the oxygen vacancies.[42,43] The distortion, as shown in Fig. 5, is enhanced in the ordered phase as the relative intensity of peak A is further lowered in spectrum (e). The decrease in peak A in spectra (d) and (e) implies that the octahedral coordination of the oxygen atoms in the modulated and ordered structure is maintained and that there is disruption of the linear Ti–O bonds at the faulted regions, owing to a strain relaxation with vacancies. The reduction of peaks C and D in spectra (d) and (e) is also associated with a higher concentration of oxygen vacancies.[44]

Additional evidence for changes in Ti valence in such $BaTiO_3$ grains comes from the observed shifts of the Ti $L_{2,3}$ edges. This is known as a chemical shift of the edge.[38] The spectra in Fig. 7(a) are normalized to the continuum interval 25 eV before the onset of the oxygen *K* edge (532 eV). The relative shift is quantified by position of the Ti L_3 onset [noted by the dashed lines in Fig. 7(a)] after placing the onset of the oxygen *K* edge at the same energy loss for all spectra. The measured energy losses are listed in Table I. No apparent chemical shift is observed from spectrum (a) to spectrum (c), implying that there is no modification to the Ti valence in the regular (defect-free) grains even in the degraded specimens. The shift of the Ti L_3 edge is about 0.8 eV down in energy between spectrum (c) to spectra (d) and (e), implying a chemical shift exists from regular $BaTiO_3$ gains to those with the modulated and ordered microstructure. A chemical shift of 0.8 eV is comparable to other titanate published results, where the shift towards lower energy loss was about 0.7 eV from the matrix to the oxygen deficient {111} twin boundary planes in a sintered bulk $BaTiO_3$.[16] Since lower oxidation states of titanium cause chemical shifts to lower energy losses,[38,45,46] this reduction in energy is likely due to the reduction of the Ti cations. Additionally, the shift of the edge onset to lower energies may be associated with the lowering of the band gap of dielectric on reduction.[47]

Leapman *et al.* defined the observed white linewidth as the FWHM of the peak and reported a L_3 width decreasing from 4.9 eV in Ti to 4.1 eV in TiO_2, implying that the $L_{2,3}$ edge width has a strong dependence on the titanium oxidation state.[38] The width changes are clearly shown in Fig. 7(b), which is an enlarged part of the Ti $L_{2,3}$ edges in Fig. 7(a). The peaks are normalized to the maximum intensity of the Ti L_2 edge. The widths of $L_{2,3}$ peaks are determined by the differences of the energy loss at half the maximum of the L_3 intensity, as shown in Fig. 7(b). The corresponding width values are listed in Table I: 9.4 eV for the regular dielectric (defect-free grains), 10 eV in the barium titanate with modulated structure, and 10.9 eV in the ordered phase. The increase in the Ti $L_{2,3}$ edge width is consistent with the presence of lower oxidation states.[45] Broadening may also result from distortion of the Ti–O octahedra, which leads to a loss in symmetry.[37,48]

The ratio of the L_3 and L_2 white line intensities is also known to be sensitive to the valence state of transition metals,[39,45,49–51] and the L_3/L_2 intensity ratio of EELS has been widely used to identify the valence state in unknown materials by comparison with standards.[52] Using Mn and Co oxides as examples, it has been found that the higher the valence of the $3d$ element, the lower the L_3/L_2 intensity ratio.[52] However, there are disagreements for the L_3/L_2 ratio for Ti and its oxides in the literature.[16,37,36,45,46,49] The calculated increase in L_3/L_2 ratios from 0.91 for higher oxidation state (Ti^{4+}) to 1.51 for lower oxidation state (Ti^{2+}) was predicted by Waddington *et al.* based on the multiconfiguration Dirac–Fock calculations.[49] However, an identical L_3/L_2 intensity ratio of 0.8:1 for both metallic Ti and TiO_2 was experimentally observed by Leapman *et al.*[38] Rečnik *et al.* reported an identical L_3/L_2 intensity ratio of 0.8 for both a $BaTiO_3$ matrix and a {111} twin boundary, although the twin plane was believed to be oxygen deficient.[16] The L_3 to L_2 white-line intensity ratio of about 0.7 was published in an EELS study of TiO_2 rutile.[37] There is only sparse literature concerning the ratio of L_3 to L_2 white-line intensity available for nonstoichiometric perovskite oxides. Although Otten *et al.* mentioned that the L_3/L_2 intensity ratio decreases with oxidation state changes when the Ti changes from Ti^{4+} in TiO_2 to Ti^{3+} in Ti_2O_3, no exact values were reported.[46] In this study, no statistically significant changes in the L_3/L_2 ratio were observed in any of the degraded regions, but we know from the observed chemical shifts of the edge onset that valence changes occurred in the modulated and long-range ordered regions.

IV. CONCLUSIONS

High spatial resolution transmission electron microscopy and electron energy loss spectroscopy are used to study newly observed planar defects in barium titanate grains in degraded BME multilayer ceramic X7R capacitors. The barium titanate in the virginal BME capacitors is slightly deficient in oxygen as it was cofired with Ni internal electrodes in a reducing atmosphere and then reoxidized at a lower temperature at a PO_2 close to the Ni/NiO equilibrium. Barium titanate X7R dielectrics have the regular perovskite crystal structure in the virginal BME capacitors. A mixture of regular and highly faulted perovskite grains is present in the degraded devices. The data indicate that the modulated and/or ordered structures are created by clustering of oxygen

vacancies in the basic structural framework of the perovskite lattice, which is therefore composed of $Ba-O_{3-x}[Vö]_x$ ($0<x<3$) instead of $Ba-O_3$ in {111} planes. The oxygen deficiencies result in local lattice distortions in the basic perovskite structure. The high concentration of oxygen vacancies is compensated electronically by valence decreases of the Ti cations in the degraded dielectrics. All the changes in the EELS spectra for the Ti $L_{2,3}$ and the O K edges are consistent with an oxygen vacancy concentration increase and a decrease in the Ti valences. The electromigration of oxygen vacancies and a reduction in the valence state of the Ti cations may play an important role in the degradation of insulation resistance of the dielectrics in degraded BME capacitors.

ACKNOWLEDGMENTS

This work has been supported in part by NSF-IUCRC Center for Dielectrics Studies (CDS) and KEMET Electronic Corporation. We also thank CDS members for useful discussions, especially Dr. H. Chazono at Taiyo Yuden Co., Ltd. in Japan and Materials Research Institute TEM facilities at the Pennsylvania State University, University Park.

[1] J. M. Herbert, *Ceramic Dielectrics and Capacitors* (Gordon and Breach, Philadelphia, 1985).
[2] S. Sumita, M. Ikeda, Y. Nakano, K. Nishiyama, and T. Nomura, J. Am. Ceram. Soc. **74**, 2739 (1991).
[3] Y. Sakabe, J. Am. Ceram. Soc. **66**, 1338 (1987).
[4] H. Kishi, Y. Mizuno, and H. Chazono, Jpn. J. Appl. Phys., Part 1 **42**, 1 (2003).
[5] T. I. Prokopowicz and A. R. Vaskas, Ferroelectrics **10**, 225 (1972).
[6] T. Baiatu, R. Waser, and K. H. Hardtl, J. Am. Ceram. Soc. **73**, 1663 (1990).
[7] D. P. Cann, J. P. Maria, and C. A. Randall, J. Mater. Sci. **36**, 4969 (2001).
[8] Y. Tsur, A. Hitomi, and C. A. Randall, Jpn. J. Appl. Phys., Part 1 **40**, 255 (2001).
[9] C. A. Randall, J. Ceram. Soc. Jpn. **109**, S2 (2001).
[10] Y. Tsur and C. A. Randall, AIP Conf. Proc. **535**, 283 (2000).
[11] R. F. Klie, Y. Ito, S. Stemmer, and N. D. Browning, Ultramicroscopy **86**, 289 (2001).
[12] S. Stemmer, A. Sane, N. D. Browning, and T. J. Mazanec, Solid State Ionics **130**, 71 (2000).
[13] S. Stemmer, A. J. Jacobson, X. Chen, and A. Ignatiev, J. Appl. Phys. **90**, 3319 (2001).
[14] A. Gloter, J. Ingrin, D. Bouchet, K. Scrivener, and C. Colliex, Phys. Chem. Miner. **27**, 504 (2000).
[15] Z. L. Wang and J. S. Yin, Philos. Mag. B **77**, 49 (1998).
[16] A. Rečnik, J. Bruley, W. Mader, D. Kolar, and M. Rühler, Philos. Mag. B **70**, 1021 (1994).
[17] C. L. Jia, K. Urban, M. Mertin, S. Hoffmann, and R. Waser, Philos. Mag. A **77**, 923 (1998).
[18] H. Chazono and H. Kishi, Jpn. J. Appl. Phys., Part 1 **40**, 5624 (2001).
[19] R. Waser and R. Hagenbeck, Acta Mater. **48**, 797 (2000).
[20] T. Hölbling and R. Waser, J. Appl. Phys. **91**, 3037 (2002).
[21] M. Opitz, J. Roubert, K. Albertson, D. Hennings, J. Beeson, and C. A. Randall, J. Am. Ceram. Soc. (to be published).
[22] D. E. Newbury, D. C. Joy, P. Echlin, C. E. Fiori, and J. I. Goldstein, *Advanced Scanning Electron Microscopy and X-Ray Microanalysis* (Plenum, New York, 1986).
[23] C. F. Li, Y. Bando, M. Nakamura, and N. Kimizuka, J. Solid State Chem. **142**, 174 (1999).
[24] E. Hamada, W. S. Cho, and K. Takayanagi, Philos. Mag. A **77**, 1301 (1998).
[25] O. Eible, P. Pongratz, and P. Skalicky, Philos. Mag. B **57**, 521 (1988).
[26] K. P. Fahey, B. M. Clemens, and L. A. Wills, Appl. Phys. Lett. **67**, 2480 (1995).
[27] C. L. Jia, K. Urba, S. Hoffmann, and R. Waser, J. Mater. Res. **13**, 2206 (1998).
[28] C. L. Jia, R. Rosenfeld, A. Thust, and K. Urban, Philos. Mag. Lett. **79**, 99 (1999).
[29] C. H. Lei, C. L. Jia, M. Siegert, and K. Urban, Philos. Mag. Lett. **80**, 371 (2000).
[30] J. W. Jang, W. J. Cho, J. H. Lee, S. S. Choi, and T. S. Hahn, Jpn. J. Appl. Phys., Part 1 **36**, 6942 (1997).
[31] C. A. Randall, S. F. Wang, D. Laubscher, J. P. Dougherty, and W. Huebner, J. Mater. Res. **8**, 871 (1993).
[32] G. Y. Yang, Y. Bando, M. Saeki, and M. Onoda, Acta Mater. **46**, 5985 (1998).
[33] N. D. Browning, D. J. Wallis, P. D. Nellist, and S. J. Pennycook, Micron **28**, 334 (1997).
[34] L. A. Grunes, R. D. Leapman, C. N. Wilker, R. Hoffmann, and A. B. Kunz, Phys. Rev. B **25**, 7157 (1982).
[35] R. F. Egerton, *Electron Energy-Loss Spectroscopy in the Electron Microscope*, 2nd ed. (Plenum, New York, 1996).
[36] V. J. Keast, A. J. Scott, R. Brydson, D. B. Williams, and J. Bruley, J. Microsc. **203**, 135 (2001).
[37] R. Brydson, H. Sauer, W. Engel, J. M. Thomas, E. Zeitler, N. Kosugi, and H. Kuroda, J. Phys.: Condens. Matter **1**, 797 (1989).
[38] R. D. Leapman, L. A. Grunes, and P. L. Fejes, Phys. Rev. B **26**, 614 (1982).
[39] S. D. Berger, J. M. Macaulay, and L. M. Brown, Philos. Mag. Lett. **56**, 179 (1987).
[40] M. Sankaraman and D. Perry, J. Mater. Sci. **27**, 2731 (1992).
[41] J. K. Burdett, *Chemical Bonding in Solids* (Oxford University Press, New York, 1995).
[42] N. D. Browning, H. O. Moltagi, and J. P. Buban, Phys. Rev. B **58**, 8289 (1998).
[43] N. D. Browning and S. J. Pennycook, J. Phys. D **29**, 1779 (1996).
[44] R. F. Klie and N. D. Browning, Appl. Phys. Lett. **77**, 3737 (2000).
[45] R. D. Leapman and L. A. Grunes, Phys. Rev. Lett. **45**, 397 (1980).
[46] M. T. Otten, B. Miner, J. H. Rask, and P. R. Buseck, Ultramicroscopy **18**, 285 (1985).
[47] R. Brydson, H. Sauer, and W. Engel, in *Transmission Electron Energy Loss Spectroscopy in Materials Science*, edited by M. M. Disko, C. C. Ahn, and B. Fultz (TMS, USA, 1991), pp. 131–154.
[48] S. Stemmer, S. K. Streiffer, N. D. Browning, and A. I. Kingon, Appl. Phys. Lett. **74**, 2432 (1999).
[49] W. G. Waddington, P. Rez, I. P. Grant, and C. J. Humphreys, Phys. Rev. B **34**, 1467 (1986).
[50] Z. L. Wang and Z. C. Kang, *Functional and Smart Materials Structural Evolution and Structural Analysis* (Plenum, New York, 1998).
[51] G. Y. Yang and J. Zhu, J. Magn. Magn. Mater. **220**, 65 (2000).
[52] See, for example, Z. L. Wang, J. S. Yin, and Y. D. Jiang, Micron **31**, 571 (2000).